A direct interaction model for chemiluminescent reactions

M. G. Prisant,[a] C. T. Rettner,[b] and R. N. Zare[c]
Department of Chemistry, Stanford University, Stanford, California 94305

(Received 30 April 1984; accepted 22 May 1984)

A fully general direct interaction with product repulsion (DIPR) model is developed to aid in the interpretation of product population and alignment data from beam-gas chemiluminescence reactions of the type: $A + BC \rightarrow AB^* + C$, where AB^* is an electronically excited diatomic product. In this model an electron jump occurs at relatively large A–BC reagent separation which initiates a strong repulsive interaction in BC. This is followed by an attractive interaction between A and B, which is less rapid than the BC repulsion. Product repulsion is taken to be distributed as in photodissociation (the DIP extension of the DIPR model), and the attractive and repulsive energy releases are considered to be separable. The electronic energy of the BC product is subtracted from the total available energy to yield an effective exothermicity which is set equal to the sum of the attractive and repulsive energies. Given reaction exothermicity, reagent and product molecular constants, and repulsive interaction parameters, this model yields the product alignment, vibrational distribution, and rotational distribution for each possible product electronic state. Application to the $Ca(^1S_0) + F_2 \rightarrow CaF(B\,^2\Sigma^+) + F$ reaction shows good agreement with experimental results. It is suggested for $Ca + F_2$ that the CaF^* alignment originates from a collinear orientational preference for reaction of the reagents.

I. INTRODUCTION

The understanding of reaction dynamics in terms of electronic structure is a major goal in the study of elementary chemical reactions. Ultimately this means being able to rationalize the molecular dynamics observed in the laboratory with trajectory calculations on a full potential surface generated by solution of the electronic Schrödinger equation. For two of the simplest bimolecular reactions $H + HH \rightarrow HH + H$ and $F + HH \rightarrow FH + H$, much progress has been achieved in all aspects—potential surface, trajectory calculations, and experimental measurements—of this ultimate explanation of chemical behavior.[1–7]

Unfortunately, the near-term prospects are not encouraging for applying this sort of rigorous approach to the vast majority of $A + BC$ systems. Even when a potential surface is available for computing trajectories, there is no guarantee that dynamical properties can be successfully predicted.[8] Mapping aspects of observed dynamical behavior to specific attributes of the surface is yet more difficult.[9] Even the best potential surface and trajectory calculations constitute only the first step in a detailed understanding of reaction mechanism in terms of electronic structure. Added to the computational and theoretical problems are the experimental difficulties involved in obtaining single-collision dynamical information on elementary molecular reactions. Finally, this experimental data, even when available, often do not directly report—due to laboratory averaging—the dynamical parameters that are necessary to make meaningful comparison between theory and experiment.

For reactions studied using the technique of electronic chemiluminescence, the theoretical approach—quasiclassical trajectories on a potential energy surface—meets all the difficulties just described exacerbated by the participation of more than one adiabatic surface in the reaction dynamics.[10] These theoretical difficulties are particularly disappointing in view of the extensive internal product state information often provided by the chemiluminescent technique.[11] For the prototype reaction $Ca(^1S_0) + F_2 + CaF(B\,^2\Sigma^+) + F$ this information includes population data via analysis of the emission spectrum and product state-resolved rotational alignment data via analysis of emission polarization.[12–15] Analysis of experimental data from these types of systems requires development of a theoretical approach appropriate in its level of rigor, simple enough to be computationally tractable, but sufficiently sophisticated to suggest an electronic structure or chemical interpretation for the dynamical information obtained.

An empirical approach that works with a highly idealized interaction potential may offer many advantages. First, the use of trajectory calculations to assist in understanding the wealth of experimental data from chemiluminescent reactions becomes practicable. Second, for a sufficiently simplified interaction potential—one that focuses on a single dominating aspect of the reaction mechanism—the calculations become relatively inexpensive from a computational point of view. This allows the investigator to explore the full ramifications of the assumed mechanism for a particular system by extensive variation of the model parameters. Such flexibility is worthwhile not only in the narrow context of the specific reaction studied but also in the broader sense of clearly pointing to how dynamical behavior may be traced to specific attributes of a potential surface. Finally, the interaction potential may be formulated in a way to make the chemical meaning of parameters transparent. This allows for better understanding of any individual system studied and facilitates the development of a general computer program applicable to a broad range of different reactions.

A promising path to an idealized interaction potential for chemiluminescent reactions is suggested by theoretical

[a] Present address: Department of Chemistry, University of Toronto, Toronto, M5S 1A1, Canada.
[b] Present address: IBM Corporation, K33/281, 5600 Cottle Road, San Jose, California 95193.
[c] Holder of a Shell Distinguished Chair.

and experimental work pertaining to the electron-jump mechanism.[16–18] This mechanism presumes that all reactive trajectories make a sudden transition at relatively large reagent separation from a covalent to an ionic surface. The behavior of trajectories on potential surfaces representative of alkali-atom halogen-molecule electron-jump reactions was studied by Polanyi and co-workers.[19,20] In these studies, initial motion on the covalent surface had negligible influence on the dynamical behavior of reactive trajectories. The repulsive energy imparted to BC as a result of this interaction tended to be released while A and B were widely separated. On this basis the magnitude of repulsion on each surface was defined by the energy required to remove C from the BC reagent bond length to infinity for collinear ABC with A at the electron-jump crossing radius. If the magnitude of repulsion, so defined, exceeded 10% of the total reaction exoergicity, then Polanyi and co-workers found that a model interaction, based on C repulsion and integrable in a single step, did very well at reproducing the product state distributions of trajectories on the full surface. This approximation, called the direct interaction with product repulsion or DIPR model,[20] draws additional empirical support from its ability to account for angular distributions in the reactions of alkali atoms with halogen molecules.[21]

Noting the striking similarity of the recoil energy distribution of halogen atoms produced by the reactions of halogen molecules with hydrogen atoms to that produced by photodissociation of halogen molecules, Herschbach and coworkers[21,22] proposed a "distributed as in photodissociation" of DIP extension to the original DIPR model: this makes the BC repulsion event in the electron jump analogous to photodissociation. The more detailed description of the electron jump contained in the DIPR-DIP provides a semiempirical basis for estimating the parameters of the repulsive interaction.[23–26]

The DIPR-DIP model[19–29] is particularly attractive for application to chemiluminescent reactions. First the main features of the electron-jump mechanism in alkali-atom halogen-molecule reactions have already been used as a point of reference in describing many chemiluminescent reactions presently under study.[11] Second, the formalism of the DIPR model collapses the electronic problem in chemiluminescent reactions to the single parameter of attractive energy release. This is because the angular momentum of the product is fixed by the early release of repulsive energy. Thus in the case where chemiluminescence is a minor process which does not perturb appreciably the ground state, it becomes possible to calculate the product internal state distributions without dealing in detail with the really sticky problems of how the reaction system reaches the final product electronic state. In this study, we consider the extension of the DIPR-DIP formalism to product population and alignment data obtained using the electronic chemiluminescence technique.

Before embarking on the development of this model we briefly remark on the conditions of its applicability. The DIPR model provides an exact description of the dynamical behavior of a single reactive trajectory on the full potential so long as the repulsive and attractive interactions are *sequential* and *separable* on the regions of the surface sampled by the trajectory. Here, sequential means that the pairwise repulsive interaction between B and C must precede the pairwise attractive interaction between A and B, and separable means that there be no interaction between A and BC during the BC repulsion and no interaction between C and AB during the AB attraction. Conditions which promote a direct mechanism and minimize the interaction of A and BC during the release of repulsive energy favor this idealization. These conditions include a large crossing radius for the electron jump, large and rapid repulsive energy release, and high reaction exoergicity. To the extent that repulsion and attraction are sequential and separable for reactive trajectories, Polanyi's work suggests that the DIPR model should provide an excellent approximation of the dynamical behavior of the full surface travelled.

By the criteria just outlined, the $Ca(^1S_0) + F_2 \rightarrow CaF(B\,^2\Sigma^+) + F$ chemiluminscent reaction is a good candidate for study using a direct interaction model. The consistency or inconsistency of product-state data with a highly repulsive intermediate resembling Ca^+F^-F cannot be predicted from general considerations.[30,31] The agreement of experimental data on this reaction with predictions from a DIPR-DIP model would argue strongly for a "reaction intermediate" resembling those of alkali-atom halide-molecule reactions rather than the complex mechanism suggested by the chemical stability of CaF_2.

II. THEORY

In this section we review the DIPR-DIP model[19–29] and recast it in a form suitable for the treatment of chemiluminescent reactions. The DIPR-DIP model can be used to calculate product vibrational and rotational energies. In addition, we show that this model can be extended to calculate product alignment as a function of internal state.

We divide the development of this section into three parts. The first part describes the DIPR potential surface appropriate to chemiluminescent reactions of the type $A + BC \rightarrow AB^* + C$. This idealized surface is based on a reaction mechanism in which a repulsive interaction in BC is initiated by an electron jump and dissipated while A and B are widely separated. Model interaction parameters and initial condition sampling distributions are developed and described. The second part describes how a direct interaction with product repulsion (DIPR) model may be used to integrate the equations of motion and to calculate product attributes. A short discussion is given on estimation of model parameters for individual reactions. The third part reviews the "distributed as in photodissociation" (DIP) extension to the DIPR model. Readers interested mainly in the application of this model may wish to go directly to Sec. III.

A. The DIPR potential

We first give a brief overview of the mode of energy release in this model. An energy level diagram for this reaction mechanism is presented in Fig. 1. It maps the relative potential energy for the various atomic configurations involved. The reagents start at infinite separation on a covalent surface. If atom A reaches the electron-jump crossing radius of diatom BC, then the reagents may cross onto an ionic

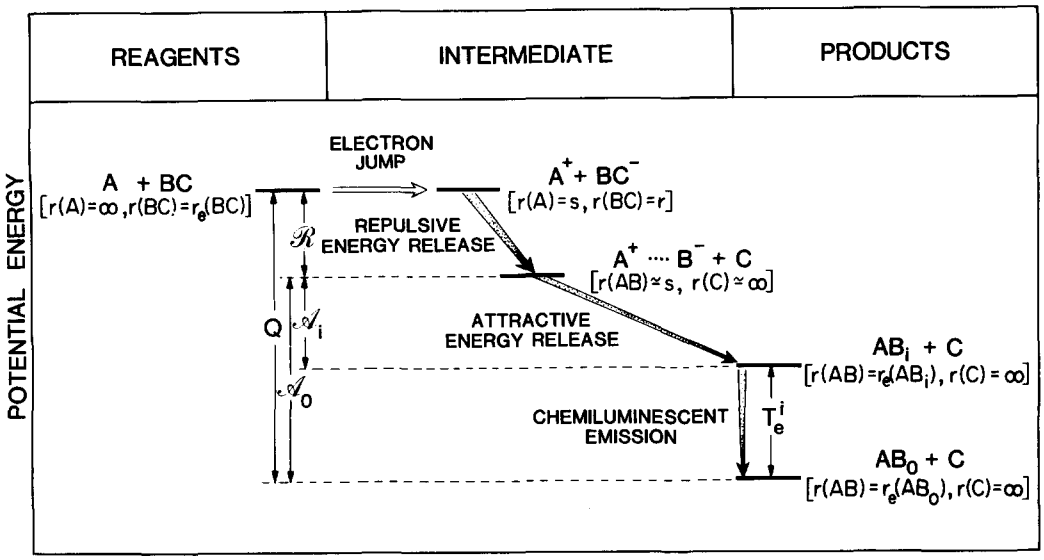

FIG. 1. Idealized potential for multisurface electron-jump reaction. For the separated reagents $r(A) = \infty$ and $r(BC) = r_e(BC)$, the equilibrium BC bond length. The switch between covalent and ionic surfaces occurs at $r(A) = s$ and $r(BC) = r$. The crossing onto the ionic surface initiates a repulsion in BC which extinguishes as $r(BC)$ lengthens. Likewise the motion of A is undeflected during repulsion and by the end of the interaction A has traveled along its original path. For the products $r(C)$ goes to infinity and the AB bond length is taken to be $r_e(AB_i)$, the equilibrium bond length for AB product in electronic state i.

surface. All reaction trajectories must make this crossing. The electron jump initiates a repulsive interaction in the resulting BC^- ion. To the extent that this interaction occurs rapidly, at large crossing radius, and imparts substantial momentum to C, then no significant forces will act on A during the release of repulsion, and B^- and C will separate rapidly to a distance beyond which no significant forces act on C. A less rapid attractive interaction follows the repulsion and brings A^+ and B^- together, as they approach the system branches to one of several product electronic states.

The DIPR potential surface is solely a function of either the paired reagent coordinates $r(A)$ and $r(BC)$ or product coordinates $r(AB)$ and $r(C)$. These are defined as follows: $r(A)$ is the distance from atom A to the center of mass of BC prior to the electron jump; $r(BC)$ is the BC bond length; $r(AB)$ is the AB bond length; and $r(C)$ is the distance from atom C to the AB center of mass. For the separated reagents, $r(A)$ is set at infinity and $r(BC)$ at $r_e(BC)$, the equilibrium bond length of ground state BC reagent. The switch between covalent and ionic surfaces occurs at $r(A) = s$ and $r(BC) = r$. The electron jump crossing radius s in Å may be calculated from Magee's well-known formula[17]

$$s = 14.4/[\text{I.P.(A)} - \text{E.A.(BC;}r)]. \quad (1)$$

Here I.P.(A) is the ionization potential in eV of A and E.A.(BC;r) is the vertical electron affinity in eV of BC at internuclear separation r. The vertical electron affinity of BC will generally vary with this BC bond length; therefore the magnitude of the crossing radius for an individual trajectory will be a function of r.

The crossing onto the ionic surface initiates a repulsive interaction in BC. The difference in the potential energy between the configurations of the electron-jump intermediates before and after the release of repulsion determines the magnitude of repulsive energy release. Because the model assumes no interaction on the covalent surface, the potential energy of the intermediate immediately prior to repulsion equals the potential energy of A removed to infinity. Likewise, because the model assumes no interaction between A and BC during the repulsion and no interaction between AB and C after the repulsion, the potential energy of the intermediate immediately after repulsion equals the potential energy of A undisplaced and C removed to infinity. On this basis, the repulsive energy is defined by

$$\mathscr{R} = V[r(A) = \infty, r(BC) = r] - V[r(A) = s, r(BC) = \infty]. \quad (2)$$

This may be estimated using the formula given by Hsu[24]

$$\mathscr{R} = \text{E.A.(B)} - \text{D(BC)} - \text{E.A.(BC;}r) \quad (3)$$

where E.A.(B) is the electron affinity of B, and D(BC) is the dissociation energy of BC (see later, Fig. 3). The magnitude of $\mathscr{R}$ will depend on the BC bond length at the time of the electron jump. Thus both repulsive energy release and electron crossing radius are coupled through the reagent vibrational phase. Lastly, the energy $\mathscr{A}$ liberated in the attractive interaction between A^+ and B^- to form the AB product in electronic state i is defined by conservation of energy:

$$\mathscr{A}(AB_i) = Q - [\mathscr{R} + T_e(AB_i)], \quad (4)$$

where $T_e(AB_i)$ is given its usual meaning as the minimum potential energy of electronic state i, and Q is the total reaction exothermicity for the production of ground state AB product (see Fig. 1).

B. Detailed description of DIPR model

1. DIPR Dynamics

A DIPR model may be used to calculate the product attributes of reactive trajectories on the idealized potential surface just described. Previous studies have developed the DIPR model for calculation of product angular distribution, rotational excitation, rotational alignment, and the correlation of rotational alignment with scattering angle.[19–29] Our treatment extends this development to product electronic vibrational excitation and the correlation of product rotational energy and alignment with vibrational state. The derivation presented here emphasizes the conservation of AB rotational angular momentum in going from the electron-jump intermediate to stable product.

We begin by describing the center-of-mass (c.m.) disposition of the system at the covalent-ionic crossing before the release of repulsive energy. Reagent BC is assumed rotation-

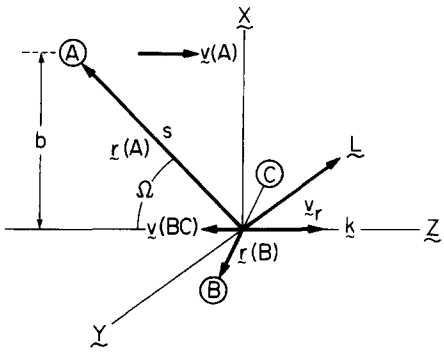

FIG. 2. DIPR model geometry. All symbols have been defined in the text.

less and vibrationless. The magnitude v_r of the relative velocity between A and BC is given by

$$v_r = [w(\mathrm{A})^2 + w(\mathrm{BC})^2 - 2w(\mathrm{A})w(\mathrm{BC})\cos\xi\,]^{1/2}, \tag{5}$$

where w(A) and w(BC) are the laboratory (LAB) speeds of A and BC, respectively, and ξ is the angle between their directions. Figure 2 shows the atomic coordinates and momenta in the space-fixed c.m. frame. The origin of the system is defined by the BC center of mass prior to the electron jump. The Z axis is chosen to lie parallel to the relative velocity direction $\hat{\mathbf{k}}$ and the Y axis antiparallel to the total reagent angular momentum L. Atom A lies at the electron-jump crossing radius in the XZ plane of the figure. The velocity of A, $\mathbf{v}$(A), points along the relative velocity vector $\hat{\mathbf{k}}$ with magnitude $[m(\mathrm{BC})/m(\mathrm{ABC})]v_r$, where m(BC) and m(ABC) are the masses of BC and A + BC, respectively. The velocity of atom B, $\mathbf{v}$(B), lies antiparallel to $\hat{\mathbf{k}}$ and has magnitude $[m(\mathrm{A})/m(\mathrm{ABC})]v_r$, where m(A) is the mass of A. The position of A is defined by the vector $\mathbf{r}$(A) of length s making the angle Ω with $\mathbf{v}$(BC). The BC bond axis is oriented arbitrarily. The three Euler angles ϕ, θ, and χ determine the relative orientation of the body-fixed frame, defined by the BC molecular axis, to the space-fixed frame. The position of atom B is defined by vector $\mathbf{r}$(B) of length $[m(\mathrm{C})/m(\mathrm{BC})]r$, where r is the BC bond length, and its direction is taken along $\hat{\mathbf{x}}$. The coordinates r_X, r_Y, r_Z of $\hat{\mathbf{x}}$ in the space-fixed frame are defined by a direction cosine transformation of $\hat{\mathbf{x}}$:

$$\begin{bmatrix} r_X \\ r_Y \\ r_Z \end{bmatrix} = \begin{bmatrix} \cos\phi\cos\theta\cos\chi - \sin\phi\sin\chi \\ \sin\phi\cos\theta\cos\chi + \cos\phi\sin\chi \\ -\sin\theta\cos\chi \end{bmatrix}. \tag{6}$$

Consider now the disposition of the system after the release of repulsive energy. The repulsive interaction occurs along the body-fixed axis $\mathbf{x}$. For repulsive energy $\mathscr{R}$, the magnitude of change in velocity of atom B along that axis will be given by

$$u = [2\mu(\mathrm{BC})\mathscr{R}]^{1/2}/m(\mathrm{B}), \tag{7}$$

where μ(BC) is the BC reduced mass. The velocity vector of B, $\mathbf{v}'$(B), at any time t after the electron jump is given by

$$\mathbf{v}'(\mathrm{B}) = \mathbf{v}(\mathrm{B}) + u\hat{\mathbf{x}} \tag{8}$$

provided that $\mathscr{R}$ has been *fully released* by this time. The position vector of B is likewise given by

$$\mathbf{r}'(\mathrm{B}) = [r(\mathrm{B}) + \eta]\hat{\mathbf{x}} - [m(\mathrm{BC})/m(\mathrm{ABC})]v_r t\hat{\mathbf{Z}}, \tag{9}$$

where η is the displacement of B along $\mathbf{x}$. The velocity of A will be unchanged by the repulsive interaction

$$\mathbf{v}'(\mathrm{A}) = \mathbf{v}(\mathrm{A}). \tag{10}$$

The position of A will be displaced along its original path according to

$$\mathbf{r}'(\mathrm{A}) = s\hat{\mathbf{r}}(\mathrm{A}) + [m(\mathrm{A})/m(\mathrm{ABC})]v_r t\hat{\mathbf{Z}}. \tag{11}$$

Thus the relative velocity of A with respect to B is

$$\begin{aligned}\mathbf{v}'(\mathrm{AB}) &= \mathbf{v}'(\mathrm{A}) - \mathbf{v}'(\mathrm{B}) \\ &= v_r\hat{\mathbf{Z}} - u\hat{\mathbf{x}}\end{aligned} \tag{12}$$

and the position of A relative to B is

$$\begin{aligned}\mathbf{r}'(\mathrm{AB}) &= r'(\mathrm{A}) - r'(\mathrm{B}) \\ &= s\hat{\mathbf{r}}(\mathrm{A}) - [r(\mathrm{B}) + \eta]\hat{\mathbf{x}} + v_r t\hat{\mathbf{Z}}.\end{aligned} \tag{13}$$

The rotational angular momentum of AB immediately following repulsion is given by

$$\begin{aligned}\mathbf{J} &= \mu(\mathrm{AB})\mathbf{r}'(\mathrm{AB})\times\mathbf{v}'(\mathrm{AB}) \\ &= \mu(\mathrm{AB})sv_r\mathbf{J}^*.\end{aligned} \tag{14}$$

Here $\mathbf{J}^*$ is defined as

$$\mathbf{J}^* = [\hat{\mathbf{r}}(\mathrm{A})\times\hat{\mathbf{Z}}] - \alpha[\hat{\mathbf{r}}(\mathrm{A})\times\hat{\mathbf{x}}] - \beta(\hat{\mathbf{x}}\times\hat{\mathbf{Z}}), \tag{15}$$

where

$$\alpha \equiv u/v_r \tag{16}$$

and

$$\beta \equiv [\eta + r(\mathrm{B}) - ut\,]/s. \tag{17}$$

The components of $\mathbf{J}^*$ may be calculated by explicitly evaluating the cross products in Eq. (15) yielding

$$\begin{bmatrix} J_X^* \\ J_Y^* \\ J_Z^* \end{bmatrix} = \begin{bmatrix} -r_Y(\alpha\cos\Omega + \beta) \\ -\sin\Omega + r_X(\alpha\cos\Omega + \beta) + r_Z(\alpha\sin\Omega) \\ -r_Y(\alpha\sin\Omega) \end{bmatrix}, \tag{18}$$

where r_X, r_Y, and r_Z are the space-fixed coordinates defined in Eq. (6). Equation (14) shows that the direction of $\mathbf{J}$ is along $\mathbf{J}^*$.

When averaged over all reagent orientations Ω, this means that the direction of $\mathbf{J}$ will be fully determined by the reduced parameters α and β. The parameter α is an energy scaling parameter such that

$$\alpha = [m(\mathrm{C})m(\mathrm{A})/m(\mathrm{B})m(\mathrm{ABC})]^{1/2}(\mathscr{R}/E_T)^{1/2}, \tag{19}$$

where E_T is the translational energy of the reagents. The significance of β may be understood by considering a repulsive force acting on B which is exponentially decaying in time. This force will be described by

$$F(t') = F(0)\exp(-t'/\tau), \tag{20}$$

where τ is the constant of decay and $F(0) = m(\mathrm{B})u/\tau$ is the force on B at the start of the repulsive interaction. The displacement η of B along $\hat{\mathbf{x}}$ is given by the integral of the velocity change along $\hat{\mathbf{x}}$:

$$\eta = \int_0^t v(t')dt', \tag{21}$$

where

$$v(t') = \int_0^{t'} F(t'')/m(\mathrm{B})dt'' = u[1 - \exp(-t'/\tau)] \quad (22)$$

is the velocity change of B along $\hat{\mathbf{x}}$ as a function of time with $v(0) = 0$ and $v(t) = u$. It follows that

$$ut - \eta = u\int_0^t t' \exp(-t'/\tau)dt', \quad (23)$$

though in our development of the DIPR model, the repulsive interaction extinguishes at time $t' = t$. To good approximation the integral in Eq. (23) may be evaluated for a rapidly decaying force by extending the upper time limit to infinity. In this case we have

$$ut - \eta = u\tau. \quad (24)$$

This means that β can be approximated by

$$\beta = [r(\mathrm{B}) - u\tau]/s. \quad (25)$$

The parameter β may now be interpreted as a position scaling parameter whose value increases with increasing BC bond length and crossing radius s and decreases with τ. To be realistically treated by the DIPR model, a reaction should be characterized by large crossing radius and rapid release of repulsion, restricting β values close to zero.

In the formulation of the DIPR model presented here, the product angular momentum is "frozen" after the release of repulsive energy because no further torques can act on the system. The rotational angular momentum of AB product thus equals—in direction and magnitude—the angular momentum calculated for AB immediately following repulsion. We therefore identify J as the rotational angular momentum of the AB product. On this basis, the product momentum and energy disposition may now be calculated.

We next consider product rotational aligment,[32] which is defined as $\langle P_2(\hat{\mathbf{J}}\cdot\hat{\mathbf{k}})\rangle$, where $\hat{\mathbf{J}}\cdot\hat{\mathbf{k}}$ is the cosine of the angle between the product angular momentum and the reagent relative velocity and $P_2(x) = (3\cos^2 x - 1)/2$. We find

$$\hat{\mathbf{J}}\cdot\hat{\mathbf{k}} = \mathbf{J}\cdot\hat{\mathbf{Z}}/J = J_Z^*/J^* = -r_Y\alpha \sin\Omega/J^*. \quad (26)$$

As α decreases, this projection goes to zero. This means that as the ratio of repulsive energy of initial translational energy decreases, AB is increasingly constrained to rotate in the XZ plane, giving a high degree of rotational alignment. Hence zero repulsion in the DIPR model corresponds to the rotationless and spinless kinematic limit[32] (RASKL) where J must lie parallel to the reagent total angular momentum L. The β parameter influences the magnitude of J but not its Z projection. Decreasing β by increasing s or decreasing τ will cause the angle between J and Z to become smaller, forcing AB to rotate in the XY plane. Conversely increasing β by increasing the internuclear separation r or decreasing the crossing radius s will cause the angle between J and Z to increase.

We now treat product rotational excitation. The magnitude of J may be used to calculate a rotational quantum number N for the AB product such that $N \simeq J/\hbar$. The rotational energy of AB will be given by

$$E_{\mathrm{rot}} = BN(N+1) - D[N(N+1)]^2, \quad (27)$$

where B is the rotational constant and D is the centrifugal distortion constant of the AB product.

Lastly, the product vibrational energy may be calculated from conservation of energy. The total energy available for excitation of AB nuclear motion in product electronic state i is given by

$$E_{\mathrm{int}} = \tfrac{1}{2}\mu(\mathrm{AB})v'(AB)^2 + \mathscr{A}(\mathrm{AB}_i) \quad (28)$$

where $\mathscr{A}(\mathrm{AB}_i)$ is the attractive energy release in going to product state i. The first term gives the energy in AB relative motion originating from reagent translation and the release of repulsive energy. The second term gives the additional energy available from AB attraction. Because of conservation of momentum, attractive energy can only go into internal and not translational AB nuclear motion. We remark that in general not all attractive energy appears as product vibration. Some must be used to overcome the centrifugal barrier encountered in the formation of AB product. The vibrational energy of AB is given by

$$E_{\mathrm{vib}} = E_{\mathrm{int}} - E_{\mathrm{rot}}. \quad (29)$$

Trajectories having E_{vib} less than the zero-point energy cannot lead to products in electronic state i.

2. Repulsive energy distribution in DIPR-DIP model

An analogy to photodissociation may be used to account for the phenomenological form of the repulsive energy distribution. The distribution of repulsive energy in direct interaction reactions is taken as originating exclusively from a Franck–Condon reflection of the BC vibrational phase distribution at the ionic-covalent crossing.

Ground vibrational state BC has a distribution of bond extensions $r(\mathrm{BC}) - r_e(\mathrm{BC})$ such that

$$P[r(\mathrm{BC})] \propto \exp\{-[r(\mathrm{BC}) - r_e(\mathrm{BC})]^2/d^2\}, \quad (30)$$

where d is the maximum displacement to the turning points of the potential. The amount of energy available for product recoil directly maps to the BC bond extension, hence the

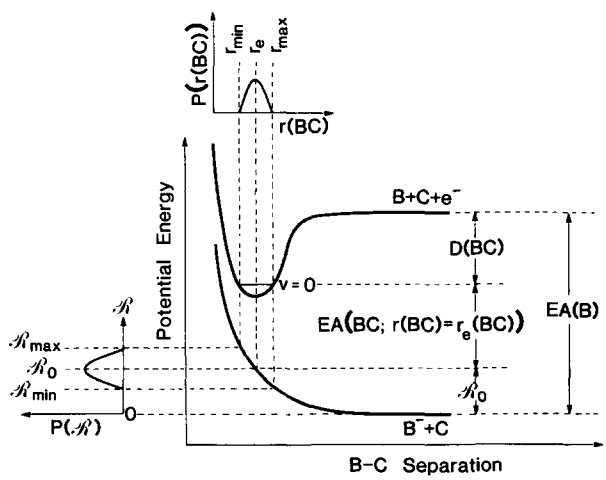

FIG. 3. Repulsive energy release in the "distributed as in photodissociation" model. A direct mapping is shown between the vibrational phase of the BC reagent and the repulsive energy released between B^- and C following the electron jump.

distribution of recoil energies mirrors that of BC displacement from the equilibrium bond length. This leads to a distribution of repulsive energies according to

$$P(\mathscr{R}) \propto \exp[-(\mathscr{R}-\mathscr{R}_0)^2/G^2] \tag{31}$$

as suggested by Herschbach.[21] Here $\mathscr{R}_0$ is the mean value of the repulsive energy [cf. Eq. (3)] and G is a measure of the width of the distribution. This picture is illustrated in Fig. 3. The slope of the potential in the region of the transition determines how strongly the repulsion varies with the BC coordinate. For the small configuration region, subtended by the turning points of the BC ground vibrational potential, the steeply decaying repulsive upper curve may be approximated as linear. The slope of the repulsive potential will then be given by $-G/d$. We may now write

$$\mathscr{R}[r(\mathrm{BC})] = \mathscr{R}_0 - (G/d)[r(\mathrm{BC}) - r_e(\mathrm{BC})], \tag{32}$$

where $\mathscr{R}[r(\mathrm{BC})]$ increases with decreasing bond extension.

These concepts may be applied to repulsive energy release in electron-jump reactions as shown in Fig. 4. The variation of $\mathscr{R}[r(\mathrm{BC})]$ in this case is due to a variation in the electron affinity of BC with internuclear distance such that[21,22]

$$\mathrm{E.A.(BC};r) = \mathrm{E.A.}[\mathrm{BC};r_e(\mathrm{BC})] + (G/d)[r(\mathrm{BC}) - r_e(\mathrm{BC})], \tag{33}$$

where the electron affinity decreases with decreasing bond length. Because the empirically determined spread in repulsive energies is taken to originate in the variation of BC electron affinity with internuclear distance, each value of $\mathscr{R}$ maps to a different value of the crossing radius

$$s(\mathscr{R}) = 14.4/\{\mathrm{I.P.(A)} - \mathrm{E.A.}[\mathrm{BC};r_e(\mathrm{BC})] + \mathscr{R}_0 - \mathscr{R}\} \tag{34}$$

and to a different value of the BC bond length

$$r(\mathscr{R}) = r_e(\mathrm{BC}) - (d/G)(\mathscr{R} - \mathscr{R}_0). \tag{35}$$

Thus higher repulsive energies originate from smaller values of BC bond length and smaller values of the crossing radius.

3. Sampling distributions

Here we consider the sampling distributions of this model in terms of the various model parameters. The angular position of the BC bond, which lies along $\hat{\mathbf{r}}(\mathrm{B})$, is determined by the three Euler angles ϕ, θ, and χ. The angle ϕ is the azimuthal orientation of $\hat{\mathbf{z}}$ in the space-fixed frame and is isotropically distributed on the interval $[0,2\pi]$. The angle θ determines the angle made by the unit vector $\hat{\mathbf{z}}$ perpendicular to the diatomic plane of rotation with the $\hat{\mathbf{z}}$ axis of a space-fixed orthogonal coordinate system. The distribution of $\cos\theta$ is equiprobable on the interval $[-1,+1]$. The angle χ determines the rotation of BC in the diatomic plane of rotation and is equiprobable on the interval $[0,2\pi]$. Let $\hat{\mathbf{r}}(\mathrm{A})$ extend from the BC center of mass to atom A. The direction of $\hat{\mathbf{r}}(\mathrm{A})$ is determined by the angle Ω it makes with the negative Z axis. This angle is related to the impact parameter b of the collision and the crossing radius s of the electron jump by

$$\sin\Omega = b/s. \tag{36}$$

The square of this quantity is taken to be equiprobable—assuming a constant opacity function—on the interval [0,1].

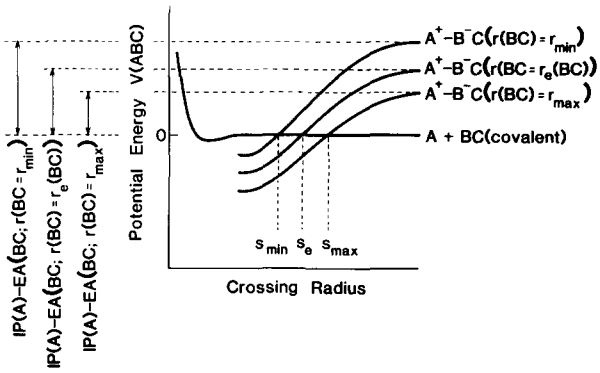

FIG. 4. Variation of the electron-jump crossing radius with the vertical electron affinity of BC, E.A.[BC;r(BC)].

An orientation dependence in the reaction mechanism may be caused by a steric factor for transmission onto the ionic surface or for branching into a particular electronic state.[11,20,33] The dynamical consequences of such efforts may be studied by switching on an orientational weighting of reagent configurations. An isotropic weighting gives each configuration identical unit weight. A weighting factor favoring collinear arrangement of reagents may be defined by

$$P[\hat{\mathbf{r}}(\mathrm{A})\cdot\hat{\mathbf{r}}(\mathrm{B})] \propto 1 + [\hat{\mathbf{r}}(\mathrm{A})\cdot\hat{\mathbf{r}}(\mathrm{B})]. \tag{37a}$$

This factor gives the perpendicular configuration half-weighting and the antiparallel configuration zero weighting. A weighting factor favoring a perpendicular arrangement may be similarly defined:

$$P[\hat{\mathbf{r}}(\mathrm{A})\cdot\hat{\mathbf{r}}(\mathrm{B})] \propto 1 - [\hat{\mathbf{r}}(\mathrm{A})\cdot\hat{\mathbf{r}}(\mathrm{B})]^2. \tag{37b}$$

This factor gives the collinear configuration zero weighting.

The repulsive energy release is chosen according to Eq. (31), where we restrict $\mathscr{R}$ to the interval $(\mathscr{R}_0 - G)$ to $(\mathscr{R}_0 + G)$. The mean repulsive energy $\mathscr{R}_0$ is obtained by substitution into Eq. (3). Approximate values of $\mathscr{R}_0$ and G for the reaction A + BC may be estimated in a semiempirical manner on the basis of atomic recoil energy distributions taken from molecular beam measurements of other electron-jump reactions involving BC or from optical absorption electron-jump reactions involving BC or from optical absorption measurements of BC photodissociation. The impulsive character of the repulsion may be judged by comparing a crude estimate[34] of the duration of BC repulsion to the vibrational period of AB. The condition that τ is less than the AB vibrational period argues that BC repulsion is not coupled to AB attraction.

Noting that in this model no forces act on the reagents before they cross onto the ionic surface the velocity characteristics of trajectories reaching the electron jump crossing are determined by strictly kinematic considerations. For the beam-gas reactions considered here, the speed of each reagent is sampled from a Boltzmann distribution determined by reagent mass and temperature. The cosine of the angle made by the beam and gas velocities, $\cos\xi$ is equiprobable on the interval [0,1]. Since the rate of reaction is proportional to the reagent relative velocity, we weight each trajectory by the magnitude of its relative velocity.

Approximate values of the model parameters for a specific chemical reaction may be determined as follows. The reaction exoergicity Q may be estimated from bond energies or obtained directly, in the case of chemiluminescent reactions, from the energy of the highest product state empirically observed.[35] An indicative, though neither mean nor central value of the crossing radius may be calculated by substituting the equilibrium or tabulated value of the BC vertical electron affinity into Eq. (1). An estimate for the mean repulsive energy $\mathscr{R}_0$ may be similarly obtained by substitution into Eq. (3). The crossing radius s_e calculated for the equilibrium bond length BC is often used to estimate the total reaction cross section $\sigma = \pi(s_e)^2$. Its comparison with the empirically determined value often serves as a rough gauge of the applicability of the electron-jump mechanism.

III. COMPUTATIONS

A. DIPR-DIP trajectories

The above model has been incorporated into a computer program which performs quasiclassical trajectory calculations on the DIPR-DIP surface.[36–38] The program calculates a reactive trajectory as follows:

(i) Initial conditions are chosen using Monte Carlo sampling, according to the distributions discussed in Sec. II B 3. Specifically, these concern the reagent velocity and orientation of the BC bond and may include the repulsive energy release, which in turn will determine the BC bond length and electron-jump crossing radius.

(ii) These conditions are applied to the equations of motion presented in Sec. II B 1 to yield the AB product rotational quantum number N, the cosine of the angle that the AB rotational angular momentum makes with the reagent relative velocity vector, and the total internal energy available to an electronically excited AB product. If the calculated value of N is greater than a carefully chosen value, set for all reactive trajectories, independent of the electronic state, then the trajectory is rejected. This cutoff only serves to define a histogram width in the sorting by N and does not constitute a dynamical constraint on the model. The upper limit should therefore be chosen to reject as few trajectories as possible. The internal energy of AB is calculated; if this is greater than the AB dissociation energy or less than the zero-point vibrational energy of the AB product in electronic state i, then the trajectory is rejected.

(iii) Using the internal energy and N the program finds the rotational and vibrational energy associated with the AB product. These rotational and vibrational energies are then converted to their reduced forms as suggested by Bernstein and Levine[39] by introducing the reduced vibrational energy

$$f = E_{\text{vib}}/[Q - T_e(\text{AB}_i)] \tag{38}$$

and the reduced rotational energy

$$g = E_{\text{rot}}/[Q - T_e(\text{AB}_i) - E_{\text{vib}}]. \tag{39}$$

Both f and g range between 0 and 1; their use greatly facilitates the description of the product state distribution.

B. Trajectory sorting

The number of events falling into each sorting category is the count in that category. The sum of event weights falling into each sorting category is the relative population in that category. Because each event will have a different weight based on its relative velocity and, possibly, its reagent orientation, the number of counts does not necessarily equal the relative population in a category. All trajectories are sorted by their rotational quantum number and by their success or failure in producing a product in electronic state i. The attributes tabulated in these sorting categories are counts, relative population, distribution mean and standard deviation. These attributes are calculated for impact parameter, energy scaling parameter, α, reagent orientation given by $\hat{\mathbf{r}}(\text{A})\cdot\hat{\mathbf{r}}(\text{BC})$, and AB alignment after repulsion given by $[3(\hat{\mathbf{J}}\cdot\hat{\mathbf{k}})^2 - 1]/2$. Reactive trajectories are (univariately) sorted by rotational quantum number N and by vibrational quantum number v. All attributes previously listed are tabulated in these categories and the distribution mean and standard deviation of the following parameters are added: the reduced vibrational energy f and the reduced rotational energy g. Two additional special sortings are made of reactive trajectories. The first is univariate sorting by g. Only relative populations are tabulated in this sorting. The second special sorting of reactive trajectories is a bivariate sorting by f and N. The attributes tabulated in this bivariate sort are counts, mean AB alignment, and its standard deviation.

C. Program implementation and running characteristics

Considerable spectroscopic data is required for the AB_i product. These should include the electronic energy T_e, the vibrational constants $\omega_e, \omega_e x_e$, the rotational constants B_e, α_e, D_e, and the dissociation energy D_e. The reagent and reaction data consist of the atomic masses m(A), m(B), m(C), the beam temperature, the gas temperature, the fundamental frequency and bond length of BC reagent, the reaction exoergicity, the highest vibrational and rotational levels populated in state i from experimental data or energy conservation, and the highest product vibrational level from energy conservation or experimentation with the calculation. The DIPR-DIP parameters required are the mean repulsive energy $\mathscr{R}_0$, the width of the repulsive energy distribution G, the crossing radius s_e for equilibrium bond length r_e(BC), and the time decay constant τ_0 for release of mean repulsive energy $\mathscr{R}_0$. Calculation options consist of: (i) orientational weighting of reagent configurations (isotropic, parallel, or perpendicular) using, e.g., Eq. (37); and (ii) the adjustment of crossing radius and BC bond length with repulsive energy according to Eqs. (34) and (35).

The DIPR program was written in Fortran and compiled in IBM Fortran H extended.[35] The program region required for execution is less than 500 kbytes. Execution time varied depending on the fraction of successful trajectories. A good benchmark of execution time on the IBM 3081 system at Stanford was 100 000 trajectories per CPU minute with approximately 20% of those successful. This allows computation of considerably more trajectories than is typical on surfaces requiring multistep integration; consequently

TABLE I. DIPR model parameters for $Ca + F_2 \rightarrow CaF(B) + F$.

Reaction exoergicity[a-c,f]	Q	$\sim 35\,000\ cm^{-1}$ (100 kcal/mol)
Electronic energy[g] of CaF(B)	T_e[CaF(B)]	$18\,841\ cm^{-1}$ (53.89 kcal/mol)
Mean repulsion[c,h]	$\mathscr{R}_0$	$\approx$(50 kcal/mol)
Repulsion width[d,h]	G	$\approx$(50 kcal/mol)
Decay constant	τ	$\sim 10^{-14}$ s
Fundamental frequency[g]	ω_e	$572.4\ cm^{-1}$
Anharmonicity[g]	$\omega_e x_e$	$31.14\ cm^{-1}$
Rotational constant[g]	B_e	$0.342\ cm^{-1}$
Vibration-rotation coupling[g]	α_e	$0.0026\ cm^{-1}$
Centrifugal distortion[g]	D_e	$4.6\times 10^{-8}\ cm^{-1}$
Equilibrium crossing radius	s_e	≈ 5 Å
Equilibrium bond length	$r_e(F_2)$	≈ 1.44 Å
Maximum vibration (products)	v_{max}	32
Maximum rotation [CaF(B)]	N_{max}	250
Maximum rotation [CaF(X)]	J_{max}	500

[a] Reference 12.
[b] Reference 13.
[c] Reference 14.
[d] Reference 21.
[e] Reference 26.
[f] Reference 35.
[g] Reference 40.
[h] Reference 41.

more cross sortings of trajectories can be made and many parameter sets tried.

IV. APPLICATION TO $Ca(^1S_0) + F_2 \rightarrow CaF(B\,^2\Sigma^+) + F(^2P)$

This section describes application of the model calculation using the extended DIPR-DIP model to the reaction of $Ca(^1S_0) + F_2 \rightarrow CaF(B\,^2\Sigma^+) + F(^2P)$. In a separate study,[15] we have made experimental measurements of the wavelength dependence of both chemiluminescent emission intensity and polarization for this reaction under single-collision beam-gas conditions. These measurements are used here for comparison with the model calculations.

Table I gives relevant data on the $Ca + F_2$ reactions and estimates for the various model parameters. We note that the magnitude, fraction and time scale[34] of repulsive energy release all favor application of the DIPR model. In this work, we use the population and alignment data from the model calculations to simulate intensity and alignment spectra. These spectra may then be directly compared with experimental results. This method has the advantage of making transparent the sensitivity of laboratory measurements to the variation of model parameters.

A. Global trends

Before going on to the variation of model parameters and the presentation of results, we note certain global trends common to the entire range of parameter values used for CaF. First, we consider those trends related to the fraction of failed (no reaction) trajectories. We find that conservation of energy and angular momentum prevent the formation of AB for some chosen values of the crossing radius, repulsive energy release, and reagent orientation. Increasing the crossing radius and repulsive energy release both lead to a higher fraction of failed trajectories in which the resulting AB angular momentum is too large for A and B to surmount the centrifugal barrier in their approach coordinate. Similarly, atom C cannot escape and no atom exchange reaction occurs. This behavior is a result of an inappropriate choice of starting conditions.

The recipe for estimating $\mathscr{R}$ described in Sec. II B 2 takes no account of centrifugal barriers present in the $A^+\cdots(BC)^-$ system following the electron jump. These modify the actual form of the repulsive energy distribution. Such effects vanish for collinear approach and become smaller with decreasing crossing radius and lower repulsive energy release. The failed trajectories modify the actual form of the repulsive energy distribution from that described in Sec. II B 2. As a conceptual aid, the trajectory program could have been equivalently structured to reject inappropriate repulsive energies according to the chosen geometry of the A–B–C system. However, this aproach would be less efficient and would not alter the predictions of the model. What *actually* occurs during a reaction of this kind is not revealed by these simplistic calculations. The conditions for an electron jump to occur do not reflect the presence of these centrifugal barriers, which only grow in height as $\mathscr{R}$ is released. Thus in reality, the reaction may indeed follow the route of our trajectories, whereby products are reflected in the exit channel to reform the reagents. However, by the time this reflection has occurred, the atoms will have assumed a new geometry and reaction or energy transfer may yet happen in a manner outside the DIPR-DIP model.

Second we consider the trends in attribute values when trajectories are sorted by vibrational level. The distribution of repulsive energies contributing to population in a given level decreases in width and mean value as v increases. A similar explanation to that just given operates. Increasing repulsion steals energy from vibration *in two ways*:

(i) It diminishes the available attractive energy which is exclusively directed along the AB coordinate and, because the rotational momentum of AB on the average increases with repulsive energy release, more of the energy which remains along the AB coordinate must be channeled into sim-

ply bringing A and B together. This limits to a low narrow range the repulsive energies which can produce highly vibrationally excited CaF.

(ii) It also limits the rotational excitation of highly vibrationally excited CaF. We also find that the product alignment increases with increasing vibrational excitation. This indicates that J is increasingly perpendicular to the relative velocity axis. Higher vibrational states also seem to originate from a more collinearly weighted distribution of reagent orientations, though in all cases the distribution is quite broad. *We thus see no evidence for a direct mapping between reagent orientation and product vibration in CaF.* The distribution of reduced impact parameters stays constant over the entire range of vibrational energies. This is a specific function of the mass ratio—here vibrational excitation is governed by repulsion. For a H + HL→HH + L reaction, we expect that this situation would reverse and reagent orientation impact parameter would play the decisive role in determining product vibrational excitation as opposed to repulsive energy release.

We experimented with varying the model parameters about central values given in Table I. Variation of the crossing radius by ± 1Å changed the fraction of failed trajectories by approximately 10%, depending on the other parameter values, but had less significant effect on the state distribution of successful trajectories. Variation of the time decay by $\pm 1\times10^{-14}$ s also was not of major significance in altering product state distributions. In subsequent calculations, the crossing radius was fixed at 5 Å and τ set to 0. *Suppression of the functional variation of crossing radius s with the repulsive energy consistently and considerably worsened the correspondence between model and experiment.* The functional variation of r and τ, however, were of minor importance. The remaining variables $\mathscr{R}$, G, and the orientational dependence all had a moderate to strong influence on the character of the model spectra, which is discussed next.

B. Effect of the mean repulsive energy

Figures 5 and 6 give the vibrational and rotational distributions predicted by the DIPR-DIP model for $\mathscr{R}_0$ values of 30, 40, 50, and 60 kcal/mol, with $\mathscr{R}_0 = G$ in every case. Table II lists the *actual* mean repulsive energy $\mathscr{R}_0'$ appropriate to these figures. These are somewhat smaller, in keeping with the arguments of Sec. IV A above. The reduced vibration and rotation population histogram bin values are denoted by bars. Each bar encompasses three model data points corresponding to each subregion in the trajectory calculation. The length of these bars may be used to estimate a deviance and thus confidence limits for the relationship of the mean value given by the Monte Carlo approximate integration to an exact integration. In this case ≃1000 reactive out of 100 000 total trajectories suffice for excellent convergence. The solid line in these and subsequent similar figures represents a least squares fit to a quartic polynomial and is intended only as a guide to the eye. Table II lists the fraction of trajectories that failed for each case.

From Figs. 5 and 6 it is seen that increasing the mean repulsive energy release correlates with a decrease in both the reduced vibrational and reduced rotational energies. The

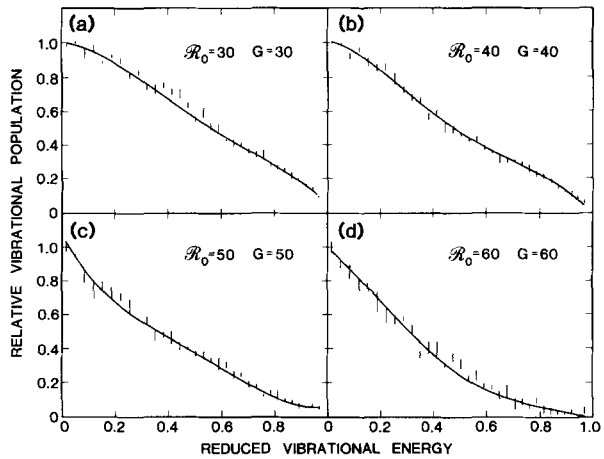

FIG. 5. Reduced vibrational energy distributions predicted by the DIPR-DIP model for $\mathscr{R}_0 = G$ with (a) $\mathscr{R}_0 = 30$ kcal/mol, (b) $\mathscr{R}_0 = 40$ kcal/mol, (c) $\mathscr{R}_0 = 50$ kcal/mol, and (d) $\mathscr{R}_0 = 60$ kcal/mol. The bars encompass the range of three separate 100 000 trajectory runs.

vibrational effect is easily understood. The vibrational energy is dominated by the attractive energy release $\mathscr{A}_i$ which falls with increasing $\mathscr{R}_0$ [see Eq. (4)]. The effect on rotation is more subtle. Here there is a tradeoff between the rotational energy and the available energy, both of which increase with $\mathscr{R}_0$. However, the increase of rotational energy is constrained by conservation of angular momentum. High rotational energies are overrepresented among the failed trajectories. The result is that the *reduced* rotational energy actually decreases with increasing $\mathscr{R}_0$.

Figure 7 displays the average product alignment as a function of reduced vibrational energy for these same four values of $\mathscr{R}_0 = G$. It is clear that those distributions are relatively insensitive to $\mathscr{R}_0$. Increasing $\mathscr{R}_0$ only serves to increase the scatter, which results from the smaller number of successful trajectories that are obtained at high $\mathscr{R}_0$ (see Table II). In all four cases the polarization increases with vibrational energy, peaking at the highest vibrational state accessed. This behavior follows from Eqs. (15) and (25), whereby large values of $\mathscr{R}$ cause the CaF angular momentum vector to depart from a plane perpendicular to the rela-

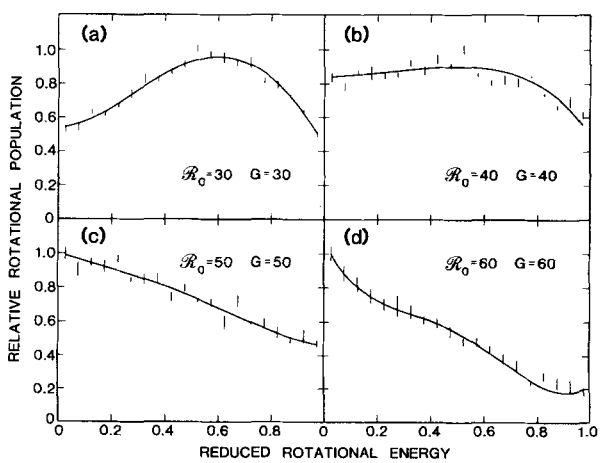

FIG. 6. Reduced rotational energy distributions predicted by the DIPR-DIP model for $\mathscr{R}_0 = G$ with (a) $\mathscr{R}_0 = 30$ kcal/mol, (b) $\mathscr{R}_0 = 40$ kcal/mol, (c) $\mathscr{R}_0 = 50$ kcal/mol, and (d) $\mathscr{R}_0 = 60$ kcal/mol. The bars encompass the range of three separate 100 000 trajectory runs.

TABLE II. Summary of DIPR-DIP trajectory parameters for $Ca + F_2 \rightarrow CaF(B) + F$.

$\mathscr{R}_0$ (kcal/mol)	G (kcal/mol)	Orientational weighting	Fraction of failed trajectories[a]	$\mathscr{R}'_0$ (kcal/mol)	Average product alignment $\langle P_2(\hat{J}\cdot\hat{k})\rangle$	Angle between Ca and F–F degrees[b]
30	30	Isotropic	0.70	20.4	−0.150	84
40	40	Isotropic	0.84	24.2	−0.149	80
50	50	Isotropic	0.92	28.5	−0.151	76
60	60	Isotropic	0.96	34.9	−0.148	70
50	25	Isotropic	0.92	39.2	−0.144	70
50	100	Isotropic	0.91	25.0	−0.154	77
50	50	Collinear	0.92	32.3	−0.167	38
50	50	Broadside	0.92	17.2	−0.098	83

[a] 100 000 trajectories run in each case.
[b] Measured with respect to the particular F atom which will bond to Ca.

tive velocity vector of the reagents. Thus maximum alignment occurs at small $\mathscr{R}$ values, which in turn are associated with the highest vibrational states. Indeed, for the highest vibrational levels populated, $\mathscr{R}$ may approach zero and maximum polarizations result. Previous experimental studies have shown that alignment does indeed increase as α decreases.[40–43]

However, a "residual" alignment has been found to persist in the limit of large α.[43] From Table II it is clear that the corresponding product-state averaged alignments are insensitive to $\mathscr{R}_0$, which leads us to suppose that these values of $\langle P_2(\hat{J}\cdot\hat{k})\rangle \approx -0.15$ refer essentially to the large α limit. The limiting anisotropy stems from a Jacobian weighting factor, proportional to $\hat{k}\cdot\hat{r}(A)$, which is generated by projecting an isotropic "dart board" of initial impact parameters onto the sphere of radius $r(A)$.[25,44]

C. Effect of repulsive energy width

To illustrate the effect of varying the width of the repulsive energy distributions we present two sets of data, obtained with $\mathscr{R}_0/G$ values of 0.5 and 2.0. These are both for $\mathscr{R}_0 = 50$ kcal/mol, which as will be discussed in Sec. IV E gives the best fit to experimental data. Figures 8 and 9 display the reduced vibrational and rotational distributions output by the model for these two cases. Again Table II lists $\mathscr{R}'_0$, the actual mean values of the repulsive energy release appropriate to the *reactive* trajectories. It is seen that increasing the width of the repulsive energy spread tends to even out the rotational distribution and reduces the slope of the vibrational distribution. This is because the spread in repulsive energy release results in a higher fraction of trajectories with both low repulsion (favoring high vibrational states) and high repulsion (favoring high rotational states).

Figure 10 shows the resulting alignment distributions with reduced vibrational energy. Again each vibrational state has a characteristic alignment, which is relatively unaffected by changes in the repulsive energy release. However, the fully averaged alignment increases from −0.144 for

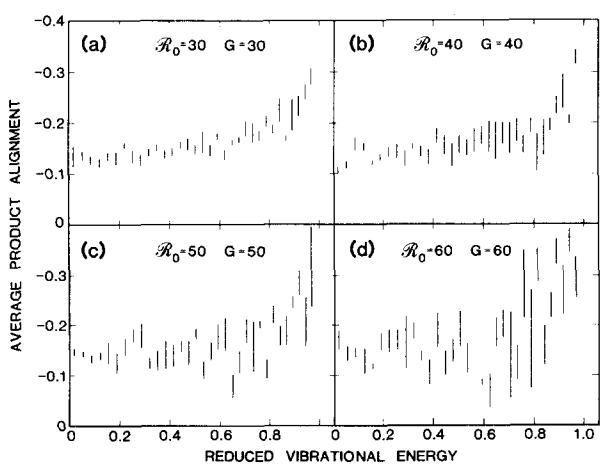

FIG. 7. Average CaF product alignment $\langle P_2(\hat{J}\cdot\hat{k})\rangle$ as a function of reduced vibrational energy calculated from the DIPR-DIP model for $\mathscr{R}_0 = G$ with (a) $\mathscr{R}_0 = 30$ kcal/mol, (b) $\mathscr{R}_0 = 40$ kcal/mol, (c) $\mathscr{R}_0 = 50$ kcal/mol, and (d) $\mathscr{R}_0 = 60$ kcal/mol. The bars encompass the range of three 100 000 trajectory runs.

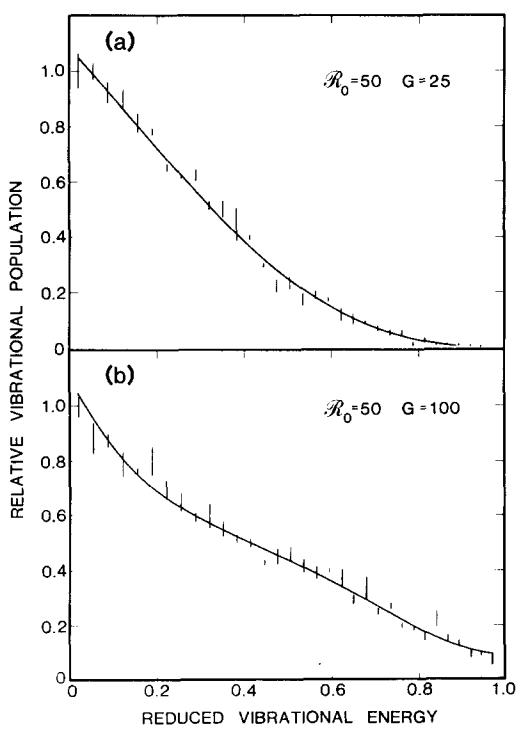

FIG. 8. Reduced vibrational energy distributions predicted by the DIPR-DIP model for (a) $\mathscr{R}_0 = 50$, $G = 25$ kcal/mol, and (b) $\mathscr{R}_0 = 50$, $G = 100$ kcal/mol.

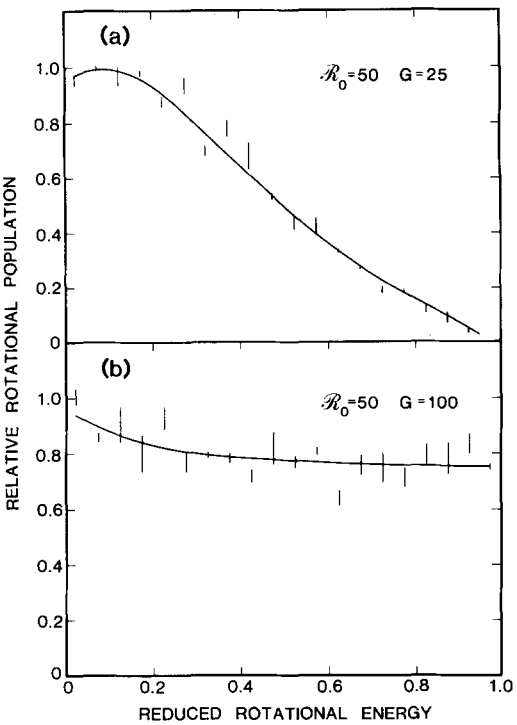

FIG. 9. Reduced rotational energy distributions predicted by the DIPR-DIP model for (a) $\mathscr{R}_0 = 50$, $G = 25$ kcal/mol, and (b) $\mathscr{R}_0 = 50$, $G = 100$ kcal/mol.

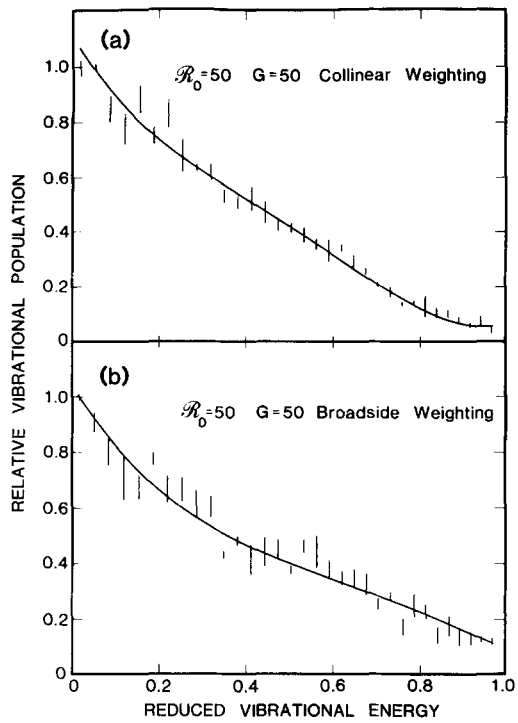

FIG. 11. Reduced vibrational energy distributions predicted by the DIPR-DIP model for $\mathscr{R}_0 = G = 50$ kcal/mol for (a) collinear weighting and (b) broadside weighting of the reagent approach geometry.

$\mathscr{R}_0/G = 2.0$ to -0.154 for $\mathscr{R}/G = 0.5$. Thus the fully averaged alignment may provide some measure of the width of the repulsive energy distribution, albeit a rather insensitive one.

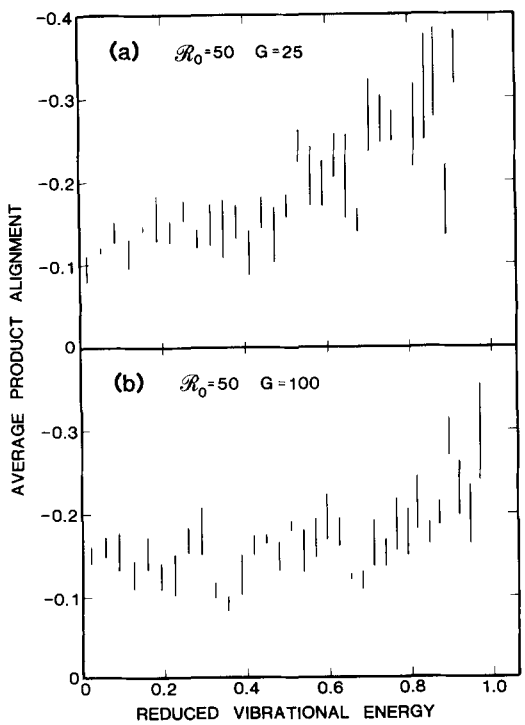

FIG. 10. Average CaF product alignment as a function of reduced vibrational energy predicted by the DIPR-DIP model for (a) $\mathscr{R}_0 = 50$, $G = 25$ kcal/mol, and (b) $\mathscr{R}_0 = 50$, $G = 100$ kcal/mol.

D. Effect of reagent orientation

When trajectories are sorted according to the quantity $\hat{\mathbf{r}}(A)\cdot\hat{\mathbf{r}}(B)$, we find that positive values are preferred. This indicates some bias towards "parallel" approach geometries. The "average" Ca–F–F angles corresponding to mean values of $\hat{\mathbf{r}}(Ca)\cdot\hat{\mathbf{r}}(F)$ are given in Table II. These show that the tendency towards parallel approach increases with increasing $\mathscr{R}_0$. [Note that both an isotropic distribution and a preference for broadside attack would yield mean values of $\hat{\mathbf{r}}(A)\cdot\hat{\mathbf{r}}(B)$ of zero, corresponding to an average angle of 90°.] This trend arises because the probability of a successful trajectory increases as the Ca–F–F angle becomes smaller (see Sec. IV A). Thus we believe that, in the absence of other steric or symmetry considerations, reactions such as Ca + F_2 will occur preferentially through geometries which are slightly closer to collinear than to broadside. This is in part a consequence of the centrifugal barrier which blocks A–B approach whenever both the crossing radius, $\mathscr{R}$ is *not* the crossing radius, but the repulsive energy release. The A–B–C angle and $\mathscr{R}$ are large.

Notwithstanding this intrinsic preference for collinear approach, we have tested two weighting factors which serve to enhance the probability of reaction for either parallel or "perpendicular" approach geometries. These weightings were given in Eqs. (7a) and (7b). Figures 11 and 12 show the resulting vibrational and rotational distributions. The vibrational distribution is found to be only weakly affected by the approach geometry. This is because the vibrational energy is governed largely by the amount of attractive energy release, which depends only on the magnitude of $\mathscr{R}$. The rotational distributions are seen to be highly sensitive to this weighting. This is expected because the magnitude of **J** is governed by

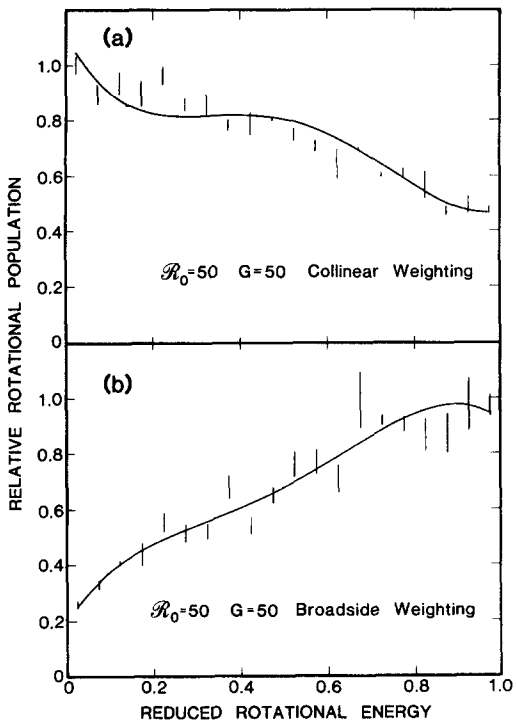

FIG. 12. Reduced vibrational energy distributions predicted by the DIPR-DIP model for $\mathscr{R}_0 = 50$ kcal/mol for (a) collinear weighting and (b) broadside weighting of the reagent approach geometry.

the lever arm that $\mathbf{v}'(B)$ makes with atom A, as is indicated by Eq. (14). Maximum $|\mathbf{J}|$ occurs when atom B flies off perpendicular to $\mathbf{r}(AB)$; a geometry favored by broadside weighting.

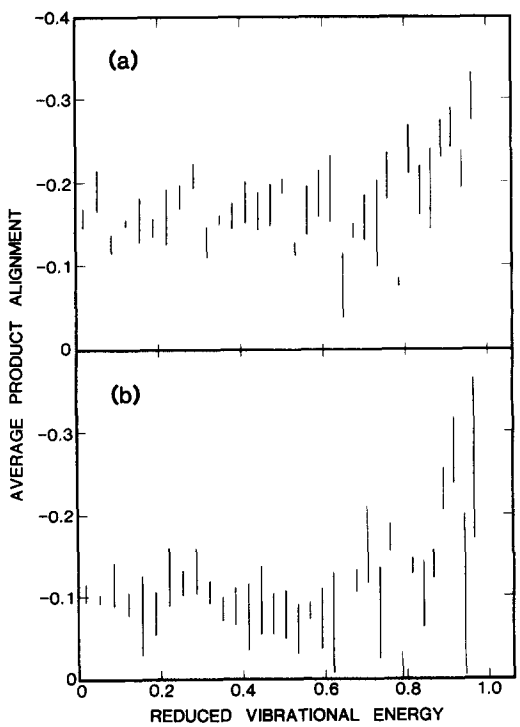

FIG. 13. Average CaF product alignment as a function of reduced vibrational energy predicted by the DIPR-DIP model for $\mathscr{R}_0 = 50$ kcal/mol for (a) collinear weighting and (b) broadside weighting of the reagent approach geometry.

Reagent orientation is also found to affect dramatically the product alignment (Fig. 13). Here we see that collinear weighting (Fig. 13c) leads to considerably higher values for the rotational polarization than broadside weighting (Fig. 13b). The vibrational state averaged alignment values are -0.167 and -0.098 for parallel and perpendicular approach, respectively. This behavior is easily understood. Reaction products are fully aligned at zero $\mathscr{R}$. Larger values can serve to "deflect" the AB angular momentum vector away from a plane perpendicular to the relative velocity vector $\mathbf{k}$. However, for close-to-collinear approaches, $\mathscr{R}$ acts roughly parallel to $\mathbf{k}$ and high polarization must result.

E. Comparison with experiment

The chemiluminescence spectrum for the reaction of Ca with F_2 was first reported in detail by Menzinger[13] and has subsequently been examined by Engelke,[14] and ourselves.[15] In the most recent study, we recorded the CaF $B\,^1\Sigma^+ - X\,^1\Sigma^+$ system at a resolution of 0.1 nm for an effusive Ca beam impinging on F_2 gas held at 77 K. This spectrum is reproduced in Fig. 14(a). In addition, we have measured the polarization at regular intervals across the spectrum, and alignment values $\langle P_2(\hat{\mathbf{J}}\cdot\hat{\mathbf{k}})\rangle$ extracted from these measurements are shown in Fig. 14(b).

In order to compare the results of the above model calculations with these observations, it is necessary to obtain sufficiently accurate spectroscopic data to permit a valid simulation of the optical spectrum. Fortunately the CaF B–X system has been carefully studied by a number of workers.[13,45,46] In particular, Menzinger[13] has provided a comprehensive set of Franck–Condon factors, while Dulick *et al.*[46] have derived a detailed set of spectroscopic constants from high resolution laser measurements. This data has been employed to produce the simulated spectra shown in Figs. 15(b) and 15(c), which are based on nascent quantum-state distributions predicted by the DIPR–DIP model.

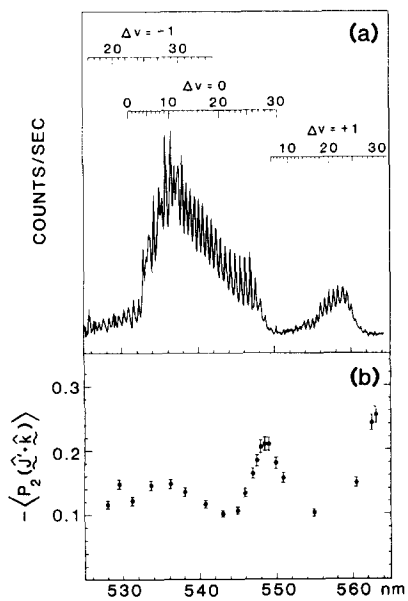

FIG. 14. Plot of (a) the $Ca + F_2 \rightarrow CaF(B\,^2\Sigma^+) + F$ chemiluminescence spectrum and (b) the $CaF(B\,^2\Sigma^+)$ product alignment as a function of wavelength. The band origin positions of the $\Delta v = 0$ sequence are indicated.

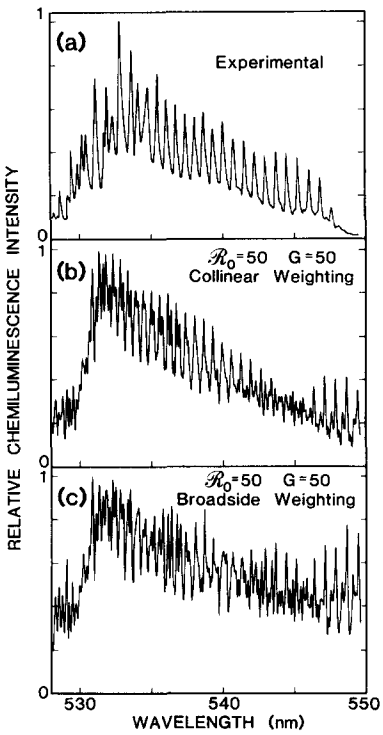

FIG. 15. Comparison of experimental and simulated CaF B–X chemiluminescence spectra: (a) observed spectrum obtained from beam-gas experiments; (b) simulated spectrum based on nascent quantum state distribution predicted by DIPR-DIP model for $\mathscr{R}_0 = G = 50$ kcal/mol with a collinear weighting factor; and (c) the same as (b) but with a broadside weighting factor.

Figure 15(b) represents the best agreement that was obtained between these model calculations and the experimental results [Fig. 15(a)]. We find that changes of about 10 kcal/mol in $\mathscr{R}_0$ and 20 kcal/mol in G discernibly degrade this agreement. Thus we believe that the quantum state distributions given in Figs. 11(a) and 12(a) closely approximate the actual nascent distributions.[47] The spectrum obtained for $\mathscr{R}_0 = G = 50$ kcal/mol but without the "parallel" weighting is not noticeably different from Fig. 15(b). This reflects the very similar product-state distributions predicted in the two cases. However, as Fig. 15(c) shows, the introduction of a perpendicular weighting factor substantially degrades the agreement between experiment and calculation. Hence we conclude that broadside approach is unfavored for this reaction.

For this reaction both Menzinger[13] and Engelke[14] have deduced vibrational distributions of the CaF B state by analysis of the B–X chemiluminescent spectrum. Unfortunately, there is substantial disagreement between these two studies. Menzinger obtained only a modest vibrational inversion, with a slight peak at $v \sim 7$, while Engelke extracted a highly inverted distribution, peaking at $v \sim 25$.

These differences are traceable to two main reasons: (i) Menzinger extracted vibrational populations by simulating the observed spectrum, while Engelke measured peak heights; and (ii) the two authors used substantially differing sets of Franck–Condon factors. Since Dulick *et al.*[46] obtain very similar Franck–Condon factors to those of Menzinger,[13] and the simulation method is expected to be much more reliable for a spectroscopically complex system such as this one, we believe that Engelke's factors may be in error.

Our vibrational distribution [Fig. 11(a)] is qualitatively similar to that of Menzinger,[13] though our results peak near $v \simeq 0$. Since the simulated spectrum agrees only poorly in the low v region (which is overlapped by the $\Delta v = -1$ bands), we feel that this discrepancy is within the limits of errors. However, we point out that if the vibrational distribution does indeed peak for $v > 0$, then the direct interaction model presented here cannot account for this feature, since all vibrational distributions that we have obtained peak at $v \simeq 0$.

Finally, we consider the alignment measurements of Fig. 14(b). Although strictly it is necessary to simulate such a spectrum for comparison with the model predictions, it is clear that the present direct interaction model can account for this behavior. For example, Figs. 7 and 13(a) display a striking resemblance to the spectral data [Fig. 14(b)]. Certainly the measured product-state averaged value of $\langle P_2(\hat{\mathbf{J}}\cdot\hat{\mathbf{k}})\rangle = -0.14 \pm 0.01$ is in excellent agreement with model predictions (see Table II), and supports the contention (Sec. IV B) that we are observing alignment values close to the large α limit,[44] where the repulsive energy release much exceeds that of reagent translational energy.

ACKNOWLEDGMENTS

M.G.P. acknowledges the cordial hospitality offered to him during his stay at the Laboratoire de Photophysique Moléculaire du CNRS, Orsay, France, made possible by the support of the U.S. National Science Foundation under NSF INT TRAVEL 79-24367. Conversations with A. Beswick, S. Leach, J. Rostas, B. Soep, and G. Taieb were particularly helpful in formulating the initial stages of this study. This work is supported by the National Science Foundation under NSF CHE 80-06524.

[1] D. G. Truhlar and R. E. Wyatt, Annu. Rev. Phys. Chem. **27**, 1 (1976).
[2] (a) G. C. Schatz and A. Kuppermann, J. Chem. Phys. **65**, 4624, 4668 (1976); (b) G. C. Schatz, J. M. Brown, and A. Kuppermann, *ibid.* **63**, 674, 685 (1975).
[3] J. T. Muckerman, *Theoretical Chemistry: Advances and Perspectives* (Academic, New York, 1981), Vol. 6, p. 1.
[4] M. Baer, Adv. Chem. Phys. **49**, 191 (1982).
[5] (a) T. P. Schaefer, P. E. Siska, J. M. Parson, F. P. Tully, Y. C. Wong, and Y. T. Lee, J. Chem. Phys. **53**, 3385 (1970); (b) R. K. Sparks, C. C. Hayden, K. Shobatake, D. M. Neumark, and Y. T. Lee, in *Horizons of Quantum Chemistry*, edited by K. Fukui and B. Pullman (Reidel, Dordrecht, 1980), p. 91.
[6] D. P. Gerrity and J. J. Valentini, J. Chem. Phys. **79**, 5202 (1983).
[7] E. E. Marinero, C. T. Rettner, and R. N. Zare, J. Chem. Phys. **80**, 4142 (1984).
[8] P. J. Kuntz, in *Atom–Molecule Collision Theory*, edited by R. B. Bernstein. (Plenum, New York, 1979).
[9] J. C. Polanyi, Faraday Discuss. Chem. Soc. **55**, 389 (1973).
[10] J. C. Tully, Comput. Chem. **5**, 159 (1981).
[11] M. Menzinger, Adv. Chem. Phys. **42**, 1 (1980).
[12] M. Menzinger, Can. J. Chem. **52**, 1658 (1974).
[13] M. Menzinger, Chem. Phys. **5**, 350 (1974).
[14] F. Engelke, Chem. Phys. **44**, 213 (1979).
[15] M. G. Prisant, C. T. Rettner, and R. N. Zare, Chem. Phys. Lett. **88**, 271 (1982).
[16] M. G. Evans and M. Polanyi, Trans. Faraday Soc. **31**, 1375 (1935).

[17]J. L. Magee, J. Chem. Phys. **8**, 687 (1940).
[18]D. R. Herschbach, Adv. Chem. Phys. **10**, 319 (1965).
[19]P. J. Kuntz, E. M. Nemeth, and J. C. Polanyi J. Chem. Phys. **50**, 4607 (1969),
[20]P. J. Kuntz, M. H. Mok, and J. C. Polanyi, J. Chem. Phys. **50**, 4623 (1969).
[21]D. R. Herschbach, Faraday Discuss. Chem. Soc. **55**, 233 (1973).
[22]R. Harris, Ph.D. thesis, Harvard University, Cambridge, Massachusetts, 1970.
[23]N. D. Weinstein, Ph.D. thesis, Harvard University, Cambridge, Massachusetts, 1972.
[24]D. S. Y. Hsu, Ph.D. thesis, Harvard University, Cambridge, Massachusetts, 1974.
[25]G. M. McClelland, Ph.D. thesis, Harvard University, Cambridge, Massachusetts, 1979.
[26]D. S. Y. Hsu, G. M. McClelland, and D. R. Herschbach, J. Chem. Phys. **61**, 4927 (1974).
[27]M. T. Marron, J. Chem. Phys. **58**, 153 (1973).
[28]P. J. Kuntz, Trans. Faraday Soc. **66**, 2980 (1970).
[29]R. N. Dixon and D. G. Truhlar, in *Atom–Molecule Collision Theory*, edited by R. B. Bernstein (Plenum, New York, 1979).
[30]S. Lu, C. A. Mims, and R. R. Herm, J. Chem. Phys. **58**, 327 (1973).
[31]D. R. Yarkony, W. J. Hunt, and H. F. Schaeffer III, Mol. Phys. **2**, 941 (1973).
[32]M. G. Prisant, C. T. Rettner, and R. N. Zare, J. Chem. Phys. **75**, 2222 (1981).
[33]R. N. Zare, Ber. Bunsenges. Phys. Chem. **78**, 153 (1974).
[34]We estimate τ as follows: approximate the repulsive potential in the region of the crossing point as $V[r(\mathrm{BC}) - r_e(\mathrm{BC})] = \mathscr{R}_0 - (G/d)[r(\mathrm{BC}) - r_e(\mathrm{BC})]$, where G is the width of the repulsive energy release and $d = [\hbar/c\omega_e(\mathrm{BC})\mu_{\mathrm{BC}})]^{1/2}$ is the maximum displacement of $r(\mathrm{BC})$ from $r_e(\mathrm{BC})$. The force acting on BC thus vanishes when $r(\mathrm{BC}) - r_e(\mathrm{BC}) = (d/G)\mathscr{R}_0$ at which point atom B has traveled a distance $\mathscr{R}_0(d/G)[m(\mathrm{C})/m(\mathrm{BC})]$. The crude average velocity of B over this distance is given by the total velocity change imparted to atom B by the repulsion. Therefore we estimate the time of the interaction by $\tau = [2\mu(\mathrm{BC})\mathscr{R}_0]^{1/2}(d/2G)$. A similar result has been obtained by Herschbach (Ref. 21) but his Eq. (5) appears to have a misprint.
[35]For full details see M. G. Prisant, Ph.D. thesis, Stanford University, Stanford, California, 1983.
[36]J. H. Halton, Soc. Ind. Appl. Math. Rev. **12**, 1 (1970).
[37]Y. A. Schreider, *Monte Carlo Methods* (Pergamon, Oxford, 1966).
[38]J. M. Hammersley and D. C. Handscomb, *Monte Carlo Methods* (Wiley, New York, 1964).
[39]R. B. Bernstein and R. D. Levine, in *Atom–Molecule Collision Theory*, edited by R. B. Bernstein (Plenum, New York, 1979), Chap. 22.
[40]C. T. Rettner and J. P. Simons, Chem. Phys. Lett. **59**, 178 (1978); Faraday Discuss. Chem. Soc. **67**, 329 (1979).
[41]J. D. McDonald, P. R. LeBreton, Y. T. Lee, and D. R. Herschbach, J. Chem. Phys. **56**, 769 (1972).
[42]R. J. Hennessy and J. P. Simons, Chem. Phys. Lett. **75**, 43 (1980).
[43]R. J. Hennessy, Y. Ono, and J. P. Simons, Mol. Phys. **43**, 181 (1981).
[44]G. M. McClelland and D. R. Herschbach, Faraday Discuss. Chem. Soc. **67**, 360 (1979).
[45]D. P. Nanda and B. S. Mohanty, Curr. Sci. **39**, 300 (1970).
[46]M. Dulick, P. F. Bernath, and R. W. Field, Can. J. Phys. **58**, 703 (1980).
[47]In separate and ongoing studies we have developed an inversion procedure for directly extracting quantum-state distributions from chemiluminescent spectra. The resulting state distributions are indeed very similar to those of Figs. 11(a) and 12(a). This work will be reported elsewhere.